

LETTER TO THE EDITOR

Cosmic-ray electron transport in the galaxy M 51

Julien Dörner^{1,2}, Patrick Reichherzer^{1,2,3}, Julia Becker Tjus^{1,2}, and Volker Heesen⁴

¹ Ruhr-Universität Bochum, Theoretische Physik IV: Plasma-Astroteilchenphysik, Universitätsstraße 150, 44801 Bochum, Germany
e-mail: jdo@tp4.rub.de

² Ruhr Astroparticle and Plasma Physics Center (RAPP Center), Ruhr-Universität Bochum, 44780 Bochum, Germany

³ IRFU, CEA, Université Paris-Saclay, F-91191 Gif-sur-Yvette, France

⁴ University of Hamburg, Hamburger Sternwarte, Gojenbergsweg 112, 21029 Hamburg, Germany

Received: June 24, 2022

ABSTRACT

Context. Indirect observations of the cosmic-ray electron (CRE) distribution via synchrotron emission is crucial for deepening the understanding of the CRE transport in the interstellar medium, and in investigating the role of galactic outflows.

Aims. In this paper, we quantify the contribution of diffusion and advection dominated transport of cosmic-ray electrons in the galaxy M51 considering relevant energy loss processes.

Methods. We use recent measurement from M51 that allow for the derivation of the diffusion coefficient, the star formation rate, and the magnetic field strength. With this input, we solve the 3D transport equation numerically including the spatial dependence as provided by the measurements, using the open-source transport framework CRPropa (v3.1). We include three-dimensional transport (diffusion and advection), and the relevant loss processes.

Results. We find that the data can be described well with the parameters from recent measurements. For the best fit, it is required that the wind velocity, following from the observed star formation rate, must be decreased by a factor of 5. We find that a model in which the inner galaxy is dominated by advective escape and the outer galaxy by diffusive one fits the data well.

Conclusions. Three-dimensional modeling of cosmic-ray transport in the face-on galaxy M51 allows for conclusions about the strength of the outflow of such galaxies by quantifying the need for a wind in the description of the cosmic-ray signatures. This opens up the possibility of investigating galactic winds in face-on galaxies in general.

Key words. astroparticle physics; diffusion; (ISM:) cosmic rays; galaxies: star formation; radiation mechanisms: non-thermal; radio continuum: galaxies

1. Introduction

In this age of multiwavelength and multimessenger astronomy, nearby galaxies that allow for spatially resolved substructures can be observed at different wavelengths in such detail that there is differential information about the population of basically all of the ingredients needed to describe spatially resolved cosmic-ray transport and interaction of cosmic rays. In particular, information on the three-dimensional magnetic field structures, a differential view on the star formation rate and secondary properties like the spectral index of cosmic rays, the cosmic-ray diffusion coefficient, as well as the advection velocity of the plasma can be provided for both edge-on (Heesen et al. 2018; Miskolczi et al. 2019; Heald et al. 2022) and face-on (Murphy et al. 2008; Tabatabaei et al. 2013; Mulcahy et al. 2016a) galaxies. This wealth of data brings one-dimensional transport models beyond their limits.

1D models try to either describe a galaxy in the edge-on or face-on geometry. Clearly, while this is a useful simplification, it neglects the true 3D structure of a galaxy. For the edge-on case, one hence neglects the local concentration of star formation such as in spiral arms where advection is more important than diffusion. Also, the conservation of magnetic flux means that at least extensions to quasi 1D models are required in order to lead to a decreasing magnetic field strength such as the ‘flux tube’ model (Heald et al. 2022). On the other hand, in face-on galaxies the radio continuum emission is smeared out in comparison with the

star formation, so that this map can be convolved to either minimize the difference between the two maps (Murphy et al. 2008) or linearize the cross-correlation between them (Berkhuijsen et al. 2013). This then will provide an estimate of the cosmic-ray diffusion length. A shortcoming of this method is that it neglects the influence of the radio halo along the line-of-sight. Also, as Mulcahy et al. (2016a) have shown, CRE escape from the galaxy cannot be neglected but is indeed required in order to explain the radio continuum spectrum. The model by Mulcahy et al. (2016a) was a first attempt to move beyond purely descriptive work in face-on galaxies, solving the diffusion-loss equation to model the radio spectral index. Obviously, the most promising way would be to go beyond this simplification and describe a galaxy with both cosmic ray diffusion and advection in a 3D model. In this paper, we use the publicly available Monte-Carlo code CRPropa (Batista et al. 2016; Merten et al. 2017; Alves Batista et al. 2021) to describe the 3D transport in M51. While originally written to describe the extragalactic transport of hadronic cosmic-rays via the solution of the equation of motion, CRPropa has been extended to a second propagation method, i.e. solving the transport equation via the approach of Stochastic Differential Equations (SDEs). The conversion of a Fokker-Planck equation into an SDE is useful here, as the particle densities are derived from the pseudo-particle trajectories. This way, the equation of motion approach and the transport equation can be treated in one framework, as both work with individual particle trajectories

(Merten et al. 2017). This approach also allows for both continuous and catastrophic losses, for the production of full particle showers in the interactions that can be followed up on, etc.

Modeling the 3D transport of CRE in M51 depends mainly on three assumptions, (1) the diffusion coefficient and its energy scaling, (2) the escape scale-height for CREs and (3) the advection speed profile. We will implement these properties in the transport code as described in the following section 2 and fit the parameters to the observed properties. The results are discussed in Section 3 and conclusions are made in Section 4.

2. Transport model

The transport of cosmic ray electrons (CREs) can be described by the diffusion-advection equation (e.g. Becker Tjus & Merten 2020)

$$\frac{\partial n}{\partial t} = D \nabla^2 n - \vec{v} \cdot \nabla n - \frac{\partial}{\partial E} \left[\frac{\partial E}{\partial t} n \right] + S, \quad (1)$$

assuming isotropic diffusion, where n is the particle density distribution, D is the diffusion coefficient, $\partial E/\partial t$ is the energy loss term described in sec. 2.1, S is the source term and \vec{v} is the advection speed derived from the star formation rate surface density (SFRD) as described in sec. 2.2. For the diffusion coefficient D we compare the observation based value $D \approx 2 \cdot 10^{28} \text{cm}^2 \text{s}^{-1}$ (Heesen et al. 2019) with the best fit model from Mulcahy et al. (2016b).

2.1. Energy loss

Energy loss terms $\partial E/\partial t$ for synchrotron emission and inverse Compton scattering are taken into account in the CRE transport equation. In our simulation we apply the energy loss as continuous process following the parametrization given by Mulcahy et al. (2016b)

$$\frac{\partial E}{\partial t} = 8 \cdot 10^{17} E^2 \left(U_{\text{rad}} + 6 \cdot 10^{11} \frac{B^2(\vec{r})}{8\pi} \right) \frac{\text{GeV}}{\text{s}}, \quad (2)$$

where E is the CRE energy in GeV, $U_{\text{rad}} = 1 \text{ eV}$ is the energy density of the interstellar radiation field and $B(\vec{r})$ is the root mean square of the magnetic field. The magnetic field model is implemented to decrease exponentially with the height z above the scale height h_b .

$$B(\vec{r}) = B(r_{\text{gc}}) \cdot \exp \left\{ -\frac{|z|}{h_b} \right\}. \quad (3)$$

Here, r_{gc} denotes the galactocentric radius and z the height above the galactic plane. The radial profile of the magnetic field strength is measured by Heesen et al. (2022, submitted) and shown in Fig. 1. The exponential cutoff scale h_b is listed in Table 1.

2.2. Source distribution

The acceleration of CREs is believed happen in star forming regions, possibly at the shock front of supernova remnants, see e.g. (Becker Tjus & Merten 2020) for a review. Therefore, we assume that the radial source position of the electrons follows the observed SFRD (see Fig. 1). The SFRD was estimated using a hybrid star-formation map from a combination of *GALEX* 156-nm far-ultraviolet and *Spitzer* 24- μm mid-infrared data (Leroy et al. 2008).

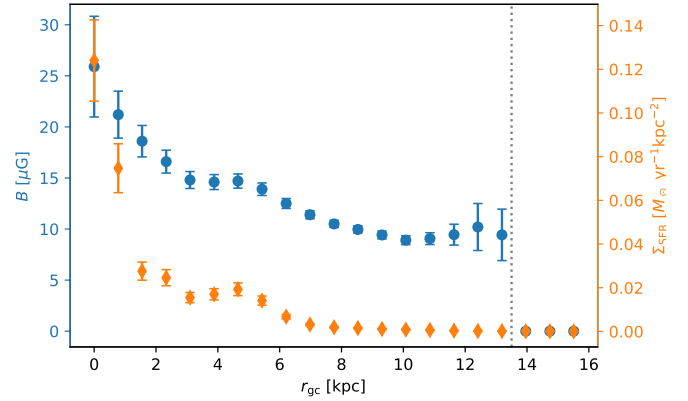


Fig. 1: Radial dependence of the root mean square of the magnetic field strength (blue) and the star formation rate (SFRD, orange). Data taken from Heesen et al. (2019) and Heesen et al. (2022, submitted). The grey dotted line indicates the restriction of our model.

2.3. Cosmic-ray advection

Even the strength of the galactic wind is assumed to be proportional to the SFRD. This is motivated both by a similarity analysis of a planar blast waves (Vijayan et al. 2020) and radio continuum observations of radio haloes in edge-on galaxies (Heesen 2021). The galactic wind speed as measured from ionised gas depends on the SFRD in a similar way on the SFRD. Hence, we use this as our parametrisation.

We take a galactic wind in z -direction $\vec{v}(\vec{r}) = \text{sgn}(z) v(r_{\text{gc}}) \vec{e}_z$, where

$$v(r_{\text{gc}}) = 10^{3.23} (\Sigma_{\text{SFR}})^{0.41} \text{ km s}^{-1} \quad (4)$$

is the best fit wind velocity following the SFRD found in Heesen et al. (2018) and sgn denotes the sign function. In this model the wind velocity does not depend on the z -position. In galactic wind models, the wind speed is zero in the galactic disc and then accelerates with height. Depending on the assumptions of geometry and energy and mass injection, this acceleration can be either gradual over a few kpc (Everett et al. 2008) or rapid over a few 100 pc (Yu et al. 2020). So far, there is no consensus for the vertical acceleration profile either as the properties of the cosmic-ray electron distribution and magnetic field strength are difficult to disentangle (Heesen 2021). Hence, we make the simplifying assumption of a constant wind speed.

2.4. CRE diffusion

Deflections of CREs in the Galactic magnetic field introduce diffusive transport behavior, which is characterized by the diffusion tensor \hat{D} that enters the transport equation. It is known that in galaxies spatial diffusion can be anisotropic or isotropic dependent on the environment (Sampson et al. 2022). In the absence of detailed knowledge for the three-dimensional modeling of diffusion tensor and their relation for M51, especially at the low particle energies, where predictions of the classical scattering relation break (Reichherzer et al. 2022b), we assume scalar diffusion. The diffusion coefficient dependency on the parameters of the CREs and the environment relies on the dominant scattering mechanism. Recent observational data, e.g., is the effective residence time of the positrons in the Milky Way, or analytical

considerations suggest energy-independent diffusion coefficients of charged particles in galaxies up to ~ 100 GeV and above. Possible explanations include advection-dominated escape (Reichherzer et al. 2022a), or transport equally contributed by both advection and diffusion (Recchia et al. 2016). However, even for diffusion-dominated escape, various explanations exist for energy-independent diffusion. Diffusion can be caused by resonant scattering of CREs in pre-existing magnetohydrodynamic turbulence or by self-excited fluctuations. At energies considered during this study, the self-excitation scenario is expected to dominate the transport properties of CREs. Waves excited through the streaming instability cause energy-independent diffusion in the absence of damping (Kempski & Quataert 2022). Energy-independence can also be achieved for particle scattering in pre-existing magnetohydrodynamic turbulence (Cowsik & Huth 2022) or through the influence of the Parker instability causing the leakage of cosmic rays out of the galaxy (Parker 1966, 1969). Also, the field-line-random walk that may contribute to perpendicular diffusion at these energies exhibits energy independent diffusion (Minnie et al. 2009; Reichherzer et al. 2020). Regardless of which of the effects or combination described above holds, we assume energy-independent diffusion. We compared our result to energy dependent diffusion which lead to a significantly worse fit for the data (see appendix B). Such a behaviour is also suggested by the 1D diffusion models of Mulcahy et al. (2016a) and the convolution experiments of Heesen et al. (2019).

2.5. Geometry of M51

To model the geometry of M51, we take a cylindrical form of the galaxy with a maximal radius of $R_{\max} = 15$ kpc and a height h_d allowing a z-position $-h_d \leq z \leq h_d$. The parameter for h_d is not fully known. Therefore, we present the results for three different models as follows:

- **[model A]** considers a large scale height for the galactic height and for the magnetic field of $h_d = h_b = 7$ kpc. This value is not realistic but chosen to see the impact of the parameter.
- **[model B]** is based on the observed synchrotron emission scale height of 1.5 kpc (Krause et al. 2018). Therefore, the height of the disk is taken to be $h_d = 3$ kpc and for the magnetic field height, we use $h_b = 6$ kpc.
- **[model C]** follows the variable scale height presented in Mulcahy et al. (2016b). Here, a scale height of $h_d = 3.2$ kpc is taken for $r_{\text{gc}} \leq 6$ kpc and $h_d = 8.8$ kpc for $r_{\text{gc}} \geq 12$ kpc. In between the scale height is interpolated linearly.

All model parameters are summarized in Table 1.

Table 1: Parameters for the magnetic field scale height h_b and the height of the disk h_d .

model	h_b	h_d
A	7 kpc	7 kpc
B	6 kpc	3 kpc
C ^a	$h = h(r_{\text{gc}})$	

Notes. ^(a) Variable scale heights as a function of the galactocentric radius as presented in Mulcahy et al. (2016b).

2.6. Simulation setup

To solve the transport equation we use the method of stochastic differential equations (SDEs) implemented in CRPropa 3.1 (Batista et al. 2016; Merten et al. 2017). We simulate 10^5 pseudo-particles in the energy range of 0.01 GeV to 50 GeV. We assume a source with a injection $dN/dE|_{\text{source}} \propto E^{-2}$. The CRE density distribution is taken for 1000 timesteps up to 500 Myr to calculate the stationary solution of the transport equation (eq. 1) following Merten et al. (2017). All particles reaching the boundary are lost to the inter galactic medium. The details of the used modules and given parameters for the simulation are given in Table 2. We analyze the CRE spectrum in the range of $0.5 \leq E/\text{GeV} \leq 6$ and fit it with a powerlaw.

3. Results

Taking the model as described before the resulting CRE spectral index is presented in Fig. 2, where the model without advection (green points) and including advection as described in sec. 2.2 (blue points) is compared for two diffusion coefficients.

In the case of the lower diffusion and neglecting advection the spectra for all models are too steep, due to the high retention time and corresponding high energy loss. Only **[model B]** undershoots the observed data in a range slightly, but it does not show the correct radial behavior. In the case of higher diffusion **[model C]** (green circle) fits the data in the inner galaxy ($r_{\text{gc}} < 6$ kpc) well. Only in the outer part of the galaxy a difference between the data and the model can be seen. This is due to different data for the magnetic field strength, starformation rate and spectral synchrotron index in Mulcahy et al. (2016b). Another point could be the difference be the 1D diffusion model used by Mulcahy et al. and the 3D approach in this work.

In the case where advection is taken into account (Fig. 2, blue points) the observed CRE spectral index is near the injection spectrum $\propto E^{-2}$. This is due to high advection speed and a quick loss of all particles. The case of the high variation for the low diffusion models in the outer galaxy can be explained by the low number of observed pseudo-particles in this domain. In this part of the galaxy the SFRD is so low, that there is nearly no production of high energy cosmic ray electrons. But due to the high advection speed the particles leave the simulation volume before they can diffuse in the outer galaxy.

Following these observation, a galactic wind significantly weaker than indicated by the SFR is necessary to match the observed data. Taking this into account we introduce a scaling factor f_{adv} in eq. (4) and optimize this value to fit the data best. Details on the optimization are given in appendix A. The final CRE indices using the optimal value for the advection normalization are shown in fig. 3. It can be seen that the lower diffusion coefficient shows a significant better fit to the data. The best fit provides **model C**. In this case the optimal normalization factor is $f_{\text{adv}} = 0.2$. The models with a constant scale height (**model A** and **model B**) does not fit the radial gradient. In the inner galaxy ($r_{\text{gc}} \lesssim 7$ kpc) are too steep and in the outer galaxy to flat.

Taking the geometry of **model C** and the lower diffusion coefficient as the best fit model analyzing the timescales shows the dominant processes. In Fig. 4 it is shown that the escape inner galaxy ($r_{\text{gc}} \lesssim 7$ kpc) is dominated by advection. The escape in the outer galaxy is dominated by diffusion. In the relevant energy range ($E > 2$ GeV) the energy loss time is much shorter than the escape timescale. This leads to a steepening of the CRE spectrum.

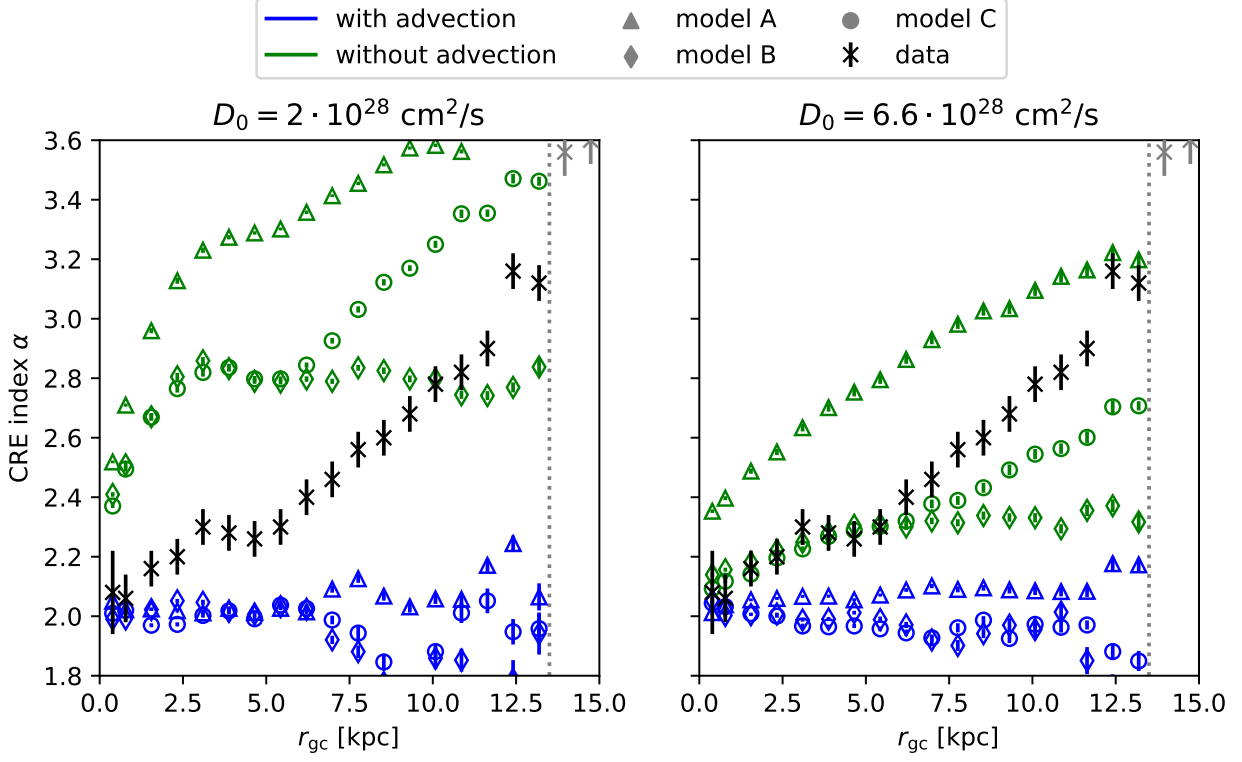


Fig. 2: CRE spectral index as a function of the galactocentric radius. The left panel shows the measured diffusion coefficient from Heesen et al. (2019) and the right panel shows the best fit value from Mulcahy et al. (2016b). The model parameters are shown in Table 1. Green points indicate simulations without advection and blue points with advection. The data are taken from Heesen et al. (2019).

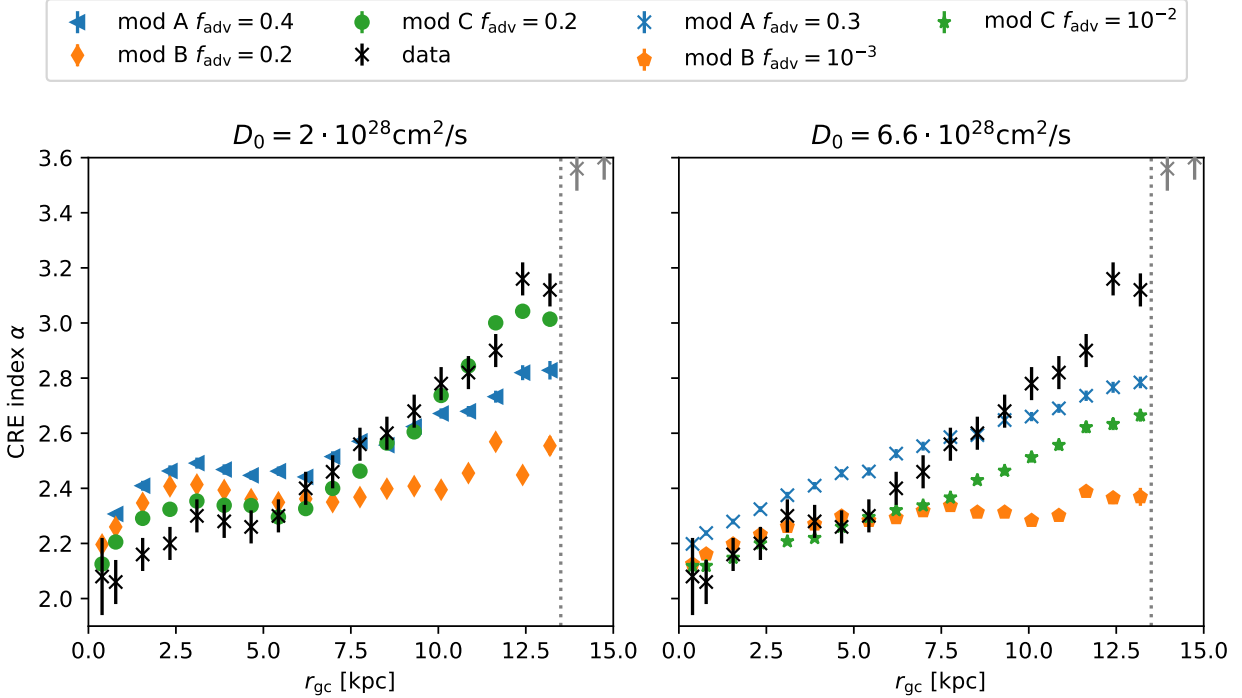


Fig. 3: Radial variation of the CRE spectral index using the optimized wind speed. The model parameters are shown in Table 1. The left panel shows the observed diffusion coefficient from Heesen et al. (2019) and the right panel the best fit value for the diffusion coefficient from Mulcahy et al. (2016b).

	module	parameters
propagation	DiffusionSDE	$l_{\min} = 0.1 \text{ pc}$, $l_{\max} = 10 \text{ kpc}$
observer	ObserverTimeEvolution	$N_{\text{step}} = 1000$, $\Delta T = 500 \text{ kyr}$
boundary	MinimumEnergy	$E_{\min} = 0.1 \text{ GeV}$
	MaximumTime	$T_{\max} = 2.5 \text{ Gyr}$

Table 2: Parameters and modules for the simulation in CRPropa3.1.

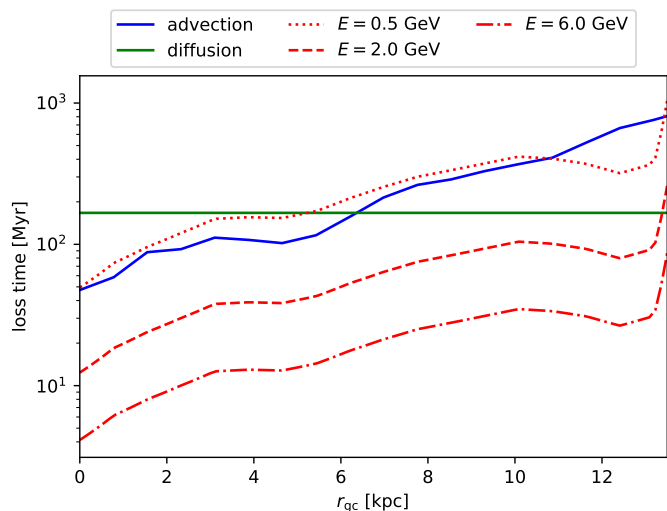


Fig. 4: Timescales for the escape via diffusion (green line) and advection (blue line) to the z-direction. Additionally the energy loss timescale is given for 3 different energy (red lines, linestyle denotes energy).

4. Conclusions

Our best-fit model to the radial gradient of the observed CRE spectra has the following settings:

1. The diffusion coefficient is independent of the energy with $D_0 = 2 \cdot 10^{28} \text{ cm}^2 \text{ s}^{-1}$. This result is in agreement with the measurement from Heesen et al. (2019).
2. The scale height for the escape of CREs depends on the galactocentric radius. We use $h_d = 3.2 \text{ kpc}$ for the inner galaxy ($r_{\text{gc}} \leq 6 \text{ kpc}$) and increase it linearly up to $h_d = 8.8 \text{ kpc}$ at $r_{\text{gc}} = 12 \text{ kpc}$.
3. The advection speed following the SFRD is reduced by a factor of 5 compared to the measurements in Heesen et al. (2018). The discrepancy can possibly be explained by the fact the radio continuum observations use global SFRD values with $\Sigma_{\text{SFR}} = \text{SFR}/(\pi r_{\star}^2)$, where r_{\star} is the radial extent of the star-forming disc. If the wind is launched from the central area of the galaxy, the SFRD would be correspondingly higher if one were to use an effective radius $r_e \approx r_{\star}/2$, this would reduce the advection speed normalisation in eq. (4) by a factor of 2. While these advection speeds may still be slightly high, the wind velocities of the ionised gas as measured by Heckman & Borthakur (2016) are in fair agreement with our new results.

We conclude that the escape of CREs is governed by different mechanisms in the inner and outer part of M51: the inner galaxy ($r_{\text{gc}} \leq 7 \text{ kpc}$) appears as an advection-dominated region, while the outer galaxy is best-described by energy-independent diffusive escape. This is basically consistent with the picture of a

wind being present. In contrast to previous results, however, our best-fit model results in a wind that is a factor of 5 smaller as derived indirectly from star-formation rate. Finally, we can show here that with a 3D transport model, it is possible to constrain the propagation environment of CREs, concerning diffusion and advection. More specifically, the 3D modeling represents an additional way of indirectly deducing the strength of a wind velocity of the face-on galaxy M51, opening the possibility to systematically investigate galactic winds for face-on galaxies in general.

Acknowledgements. JD, PR, and JBT acknowledge the support from the Deutsche Forschungsgemeinschaft, DFG via the Collaborative Research Center SFB1491 *Cosmic Interacting Matters - From Source to Signal*.

Part of this work was supported by the DFG project number Ts 17/2–1.

This work was made possible by the following software packages: `dask` (Rocklin 2015), `ipython` Pérez & Granger (2007), `matplotlib` (Hunter 2007), `numpy` (Harris et al. 2020) and `pandas` (Wes McKinney 2010).

References

- Alves Batista, R., Becker Tjus, J., Dörner, J., et al. 2021, in Proceedings of 37th International Cosmic Ray Conference — PoS(ICRC2021), Vol. 395, 978
- Batista, R. A., Dundovic, A., Erdmann, M., et al. 2016, *Journal of Cosmology and Astroparticle Physics*, 2016, 038
- Becker Tjus, J. & Merten, L. 2020, *Phys. Rep.*, 872, 1
- Berkhuijsen, E. M., Beck, R., & Tabatabaei, F. S. 2013, *MNRAS*, 435, 1598
- Cowsik, R. & Huth, D. 2022, *Advances in Space Research*, <https://doi.org/10.1016/j.asr.2022.03.010>
- Everett, J. E., Zweibel, E. G., Benjamin, R. A., et al. 2008, *ApJ*, 674, 258
- Harris, C. R., Millman, K. J., van der Walt, S. J., et al. 2020, *Nature*, 585, 357
- Heald, G. H., Heesen, V., Sridhar, S. S., et al. 2022, *MNRAS*, 509, 658
- Heckman, T. M. & Borthakur, S. 2016, *ApJ*, 822, 9
- Heesen, V. 2021, *Ap&SS*, 366, 117
- Heesen, V., Buie, E. I., Huff, C. J., et al. 2019, *A&A*, 622, A8
- Heesen, V., Krause, M., Beck, R., et al. 2018, *MNRAS*, 476, 158
- Hunter, J. D. 2007, *Computing in Science & Engineering*, 9, 90
- Kempski, P. & Quataert, E. 2022, *MNRAS*, 514, 657
- Krause, M., Irwin, J., Wiegert, T., et al. 2018, *A&A*, 611, A72
- Leroy, A. K., Walter, F., Brinks, E., et al. 2008, *AJ*, 136, 2782
- Merten, L., Becker Tjus, J., Fichtner, H., Eichmann, B., & Sigl, G. 2017, *J. Cosmology Astropart. Phys.*, 2017, 046
- Minnie, J., Mattheaus, W. H., Bieber, J. W., Ruffolo, D., & Burger, R. A. 2009, *Journal of Geophysical Research (Space Physics)*, 114, A01102
- Miskolczi, A., Heesen, V., Horellou, C., et al. 2019, *A&A*, 622, A9
- Mulcahy, D. D., Fletcher, A., Beck, R., Mitra, D., & Scaife, A. M. M. 2016a, *A&A*, 592, A123
- Mulcahy, D. D., Fletcher, A., Beck, R., Mitra, D., & Scaife, A. M. M. 2016b, *A&A*, 592, A123
- Murphy, E. J., Helou, G., Kenney, J. D. P., Armus, L., & Braun, R. 2008, *ApJ*, 678, 828
- Parker, E. N. 1966, *ApJ*, 145, 811
- Parker, E. N. 1969, *Space Sci. Rev.*, 9, 651
- Pérez, F. & Granger, B. E. 2007, *Computing in Science and Engineering*, 9, 21
- Recchia, S., Blasi, P., & Morlino, G. 2016, *MNRAS*, 462, L88
- Reichherzer, P., Becker Tjus, J., Zweibel, E. G., Merten, L., & Poeschel, M. J. 2020, *MNRAS*, 498, 5051
- Reichherzer, P., Merten, L., Dörner, J., et al. 2022a, *SN Applied Sciences*, 4, 15
- Reichherzer, P., Tjus, J. B., Zweibel, E. G., Merten, L., & Poeschel, M. J. 2022b, *MNRAS*
- Rocklin, M. 2015, in Proceedings of the 14th Python in Science Conference, ed. K. Huff & J. Bergstra, 130–136
- Sampson, M. L., Beattie, J. R., Krumholz, M. R., et al. 2022, *arXiv e-prints*, arXiv:2205.08174
- Tabatabaei, F. S., Schinnerer, E., Murphy, E. J., et al. 2013, *A&A*, 552, A19
- Vijayan, A., Nath, B. B., Sharma, P., & Shchekinov, Y. 2020, *MNRAS*, 492, 2924
- Wes McKinney. 2010, in Proceedings of the 9th Python in Science Conference, ed. Stéfan van der Walt & Jarrod Millman, 56–61
- Yu, B. P. B., Owen, E. R., Wu, K., & Ferreras, I. 2020, *MNRAS*, 492, 3179

Appendix A: optimization of the wind speed

Starting with the simulation results from the best fit wind velocity in fig. 2 can be seen that the escape due to advection is far to high to match the observed data. Therefore we introduce a normalization factor f_{adv} in eq. 4, so the advection velocity reads as

$$\vec{v}(\vec{r}) = f_{\text{adv}} \cdot 10^{3.23} \text{ km/s} (\Sigma_{\text{SFR}})^{0.41} \vec{e}_z \quad . \quad (\text{A.1})$$

To quantify the quality of the fit of the simulation results to the data a χ^2 variable

$$\chi_{\text{red}}^2 = \frac{1}{df} \sum_{i=1}^N \frac{(\alpha_{\text{sim},i} - \alpha_{\text{obs},i})^2}{\sigma_{\text{obs},i}} \quad (\text{A.2})$$

is used, where α_i denotes the spectral index in the i -th bin, σ_i is the error of the observed data and $df = N - 1$ is the degree of freedom. Here only data for $r_{\text{rg}} < 13.5$ kpc are taken into account, because the magnetic field vanishes for higher values (see fig. 1).

Trying to fit the observed data best we tried values for f_{adv} between 0.1 and 1 in steps of $\Delta f = 0.1$. Additionally we test $f_{\text{adv}} = 10^{-2}, 10^{-3}, 10^{-4}$ to compare the expected behavior for low normalization factors.

The results are shown in fig. A.1 for all 3 models and both diffusion coefficients. It can be seen that the **model C** leads to a sharp global minimum. To reach a minimized $\chi_{\text{red}}^2 \leq 1$ only small deviation for wind speed fraction about $f_{\text{adv}} = 0.2 \pm 0.1$ are allowed. This can also be seen in fig. A.2 where the spectral index is plotted against the galacto centric radius for different advection speed fractions f_{adv} . Only the values of $f_{\text{adv}} = 0.2 \pm 0.1$ are in reasonable agreement with the data (black cross).

The simulation for the higher diffusion coefficient $D_0 = 6.6 \cdot 10^{28} \text{ cm}^2/\text{s}$ do not show a plausible minimum for **model A** and **model B**. This is expected due to the fact that the value of the diffusion coefficient is fitted to match the escape timescale for the CREs in [Mulcahy et al. \(2016b\)](#). Therefore, any additional contribution of a galactic wind will lead to shorter escape timescales and a flatter spectrum. The best fit values for the wind speed fraction are shown in table A.1.

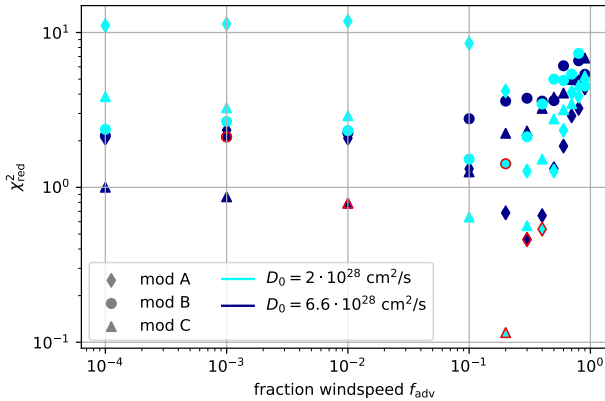


Fig. A.1: Optimization value χ_{red}^2 depending on the fraction of the wind speed f_{adv} . The minimal value is marked with a red edge of the datapoint.

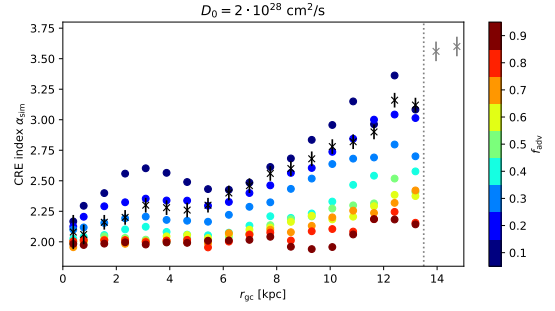


Fig. A.2: CRE spectral index for different wind speed f_{adv} (color coded) in the **model C**.

Diffusion coefficient	model A	model B	model C
$2 \cdot 10^{28} \text{ cm}^2/\text{s}$	0.2	0.4	0.2
$6.6 \cdot 10^{28} \text{ cm}^2/\text{s}$	10^{-2}	10^{-3}	0.3

Table A.1: Optimal value for the normalization of the wind speed f_{adv} in the different models.

Appendix B: energy dependent diffusion

Although the observation indicates an energy independent diffusion coefficient, we compare our model taking an energy dependence into account. In this chapter we restrict our geometry only to the best fit model [**model C**], with the radial dependent scale height. The optimization of the wind speed is performed as presented in appendix A. We compare to different diffusion models. The first model assumes a diffusion coefficient similar to the observation in the Milky Way assuming a Kolmogorov-like turbulence scaling the Diffusion reads as

$$D^I(E) = 6.1 \cdot 10^{28} \text{ cm}^2/\text{s} (E_{4\text{GeV}})^{\frac{1}{3}} \quad , \quad (\text{B.1})$$

where $E_{4\text{GeV}}$ is the energy in units of 4 GeV. As a second compare we norm the diffusion coefficient to the observed value of $D_0 = 2 \cdot 10^{28} \text{ cm}^2/\text{s}$ taking the same energy scaling as before. In this case, the diffusion coefficient reads as

$$D^{II}(E) = 2 \cdot 10^{28} \text{ cm}^2/\text{s} (E_{4\text{GeV}})^{\frac{1}{3}} \quad . \quad (\text{B.2})$$

The resulting CRE spectra are shown in fig. B.1. Both cases fit significantly worse to the data. Especially in the inner galaxy the flat spectra can not be reproduced by the energy dependent diffusion.

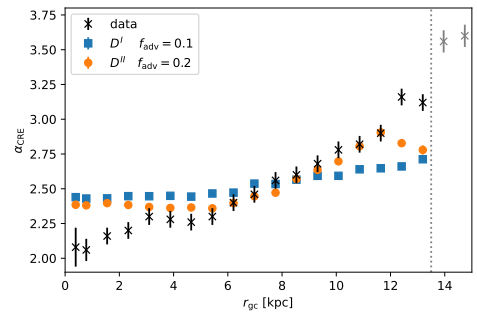


Fig. B.1: CRE spectral index for the energy dependent diffusion models using the geometry of **model C**.